A New Electron Transport Mechanism in Mitochondrial Steroid Hydroxylase Systems Based on Structural Changes upon the Reduction of Adrenodoxin†

Dirk Beilke,⊥ Roland Weiss,⊥ Frank Löhr,⊥ Primož Pristovšek,⊥,‡ Frank Hannemann,§ Rita Bernhardt,§ and Heinz Rüterjans*,⊥

Institute of Biophysical Chemistry, Johann Wolfgang Goethe-University, Biocentre N230, Marie-Curie-Strasse 9, D-60439 Frankfurt am Main, Germany and Universität des Saarlandes, Fachrichtung 8.8-Biochemie, Postfach 15 11 50, D-66041 Saarbrücken, Germany

Received December 12, 2001; Revised Manuscript Received April 17, 2002

ABSTRACT: The adrenal ferredoxin (adrenodoxin, Adx) is an acidic 14.4-kDa [2Fe-2S] ferredoxin that belongs to the vertebrate ferredoxin family. It is involved in the electron transfer from the flavoenzyme NADPH-adrenodoxin-reductase to cytochromes P-450$_{scc}$ and P-450$_{11\beta}$. The interaction between the redox partners during electron transport has not yet been fully established. Determining the tertiary structure of an electron-transfer protein may be very helpful in understanding the transport mechanism. In the present work, we report a structural study on the oxidized and reduced forms of bovine adrenodoxin (bAdx) in solution using high-resolution NMR spectroscopy. The protein was produced in *Escherichia coli* and singly or doubly labeled with ^{15}N or ^{13}C/^{15}N, respectively. Approximately 70 and 75% of the ^{15}N, ^{13}C, and ^{1}H resonances could be assigned for the reduced and the oxidized bAdx, respectively. The secondary and tertiary structures of the reduced and oxidized states were determined using NOE distance information. $^{1}H_N$-T_1 relaxation times of certain residues were used to obtain additional distance constraints to the [2Fe-2S] cluster. The results suggest that the solution structure of oxidized Adx is quite similar to the X-ray structure. However, structural changes occur upon reduction of the [2Fe-2S] cluster, as indicated by NMR measurements. It could be shown that these conformational changes, especially in the C-terminal region, cause the dissociation of the Adx dimer upon reduction. A new electron transport mechanism proceeding via a modified shuttle mechanism, with both monomers and dimers acting as electron carriers, is proposed.

Bovine adrenal-ferredoxin (bovine adrenodoxin, bAdx in the following)[1] is a 14.4-kDa [2Fe-2S] ferredoxin that belongs to the vertebrate ferredoxin family whose members exhibit a high degree of sequence homology (*1*, *2*). Bovine adrenodoxin is involved in the electron transfer from the flavoenzyme NADPH-adrenodoxin-reductase (AdR) to the cytochromes P-450$_{scc}$ and P-450$_{11\beta}$. It is part of the mitochondrial electron transport chain that is responsible for the production of steroid hormones in mammals, and is located in the adrenals (*3*) and several other tissues including brain (*4*), placenta (*5*), gonads (*6*), and liver (*7*−*9*) (in low amounts).

Four mechanisms of electron transfer (ET) have been suggested so far (*10*−*14*). According to the shuttle model, bAdx serves as a mobile carrier between AdR and Cyt P450 (*10*, *11*) (Figure 1). Other models propose a ternary (1:1:1) (*12*) and a quarternary complex (1:2:1) (*13*). The fourth model (*14*) starts from an Adx dimer which transports either one or two electrons. According to the latter model, ET can take place according to the 1:2:1 as well as the shuttle model (Figure 1). It is, however, possible that different mechanisms are active in different redox systems.

Bovine adrenodoxin has 128 amino acid residues with five cysteines at positions 46, 52, 55, 92, and 95. Four of the cysteines provide the ligation of the [2Fe-2S] cluster. The fifth cysteine, Cys95, has a free sulfur−hydrogen group (*15*).

In the oxidized state, both irons in the iron−sulfur cluster are high-spin Fe(III) and are antiferromagnetically coupled in the ground state ($S = 0$). This accounts for the paramagnetism of oxidized bovine adrenodoxin at physiological temperatures (*16*−*20*) that causes broadening of the line widths and interferes with nuclear Overhauser effect (NOE) studies. In the reduced state ($S = {}^1/_2$), one iron is Fe(II) and the other is Fe(III), and paramagnetic effects are observed at all temperatures.

Bovine adrenodoxin has been the subject of X-ray studies for more than 20 years (*14*, *21*−*24*). Up to now, two X-ray structures have been published (*14*, *22*), one of them of a shortened construct ranging from amino acid residues 4−108 (*22*)]. Conventional ^{1}H NMR spectroscopy has been utilized to study full-length bovine adrenodoxin (*25*−*28*).

† A grant from the Deutsche Forschungsgemeinschaft is gratefully acknowledged (SFB 474, P 10; Be 1343/12-1).

* To whom correspondence should be addressed. Tel.: +49-69 798 296 30. Fax: +49-69 798 296 32. E-mail: hruet@bpc.uni-frankfurt.de.

⊥ Johann Wolfgang Goethe-University.

§ Universität des Saarlandes.

‡ Present address: National Institute of Chemistry, Hajdrihova 19, 1115 Ljubljana, Slovenia.

[1] Abbreviations: AdR, NADPH-adrenodoxin-reductase; bAdx, bovine adrenodoxin; CSI, chemical shift index; ET, electron transfer; Adx(ox), Adx in the oxidized state; Adx(red), Adx in the reduced state; HSQC, heteronuclear single quantum correlation; NOE, nuclear Overhauser effect; NOESY, nuclear Overhauser and exchange spectroscopy; RMSD, root-mean-square deviation; TOCSY, total correlation spectroscopy.

10.1021/bi0160361 CCC: $22.00
Published on Web 05/25/2002

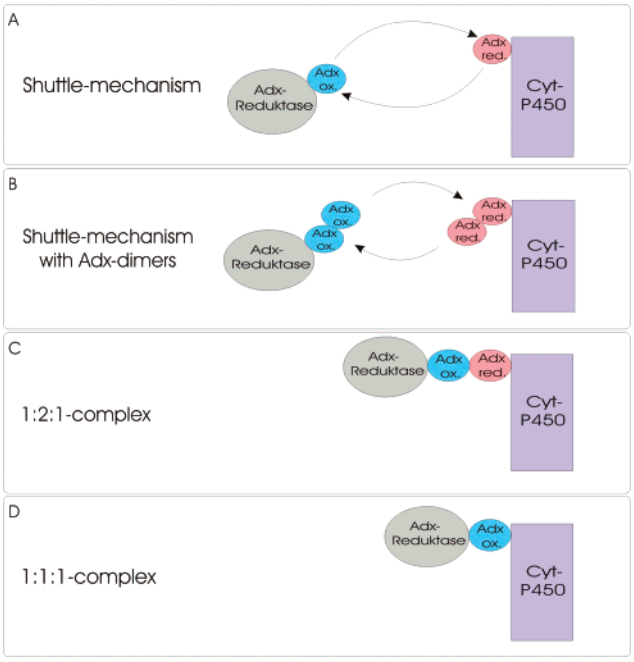

FIGURE 1: Electron transport mechanisms from the literature: (A) The shuttle model where a Adx monomer serves as mobile carrier between Adr and Cyt P450 (*10*, *11*); (B) Modified shuttle model in which Adx dimers serve as electron carrier (*14*). In models (C) and (D), a ternary and a quarternary complex is proposed (*12*, *13*).

We have recently described the sequence-specific assignments of the ^{15}N, $^{13}C'$, $^{13}C^{ali}$, $^{1}H^{ali}$, and $^{1}H^{N}$ resonances for oxidized bovine adrenodoxin (*29*). In the present work, the sequence-specific assignments for reduced bAdx were determined, and the secondary and tertiary structures of the protein in both oxidation states were investigated. It was shown that redox-dependent changes of the C-terminus not only exercises an influence on the binding to the cytochrome but is also responsible for the dissociation of the adrenodoxin dimer that exists in the oxidized state. A new electron transport mechanism is suggested based on structural changes upon reduction and on investigations of the reduced state at low concentrations.

EXPERIMENTAL PROCEDURES

Chemicals. $^{15}NH_4Cl$, $^{13}C_6$-D-glucose (fermentation grade), and $^{13}C_3$-glycerol were purchased from Martek (Martek Biosciences Corp., Columbia, MD). Sodium dithionite was purchased from Sigma-Aldrich (Germany).

Protein Expression and Purification. Bovine adrenodoxin was produced in *Escherichia coli* strain BL21 by using the plasmid pKKHC/bAdx with the strong trc-promotor as described previously (*30*). The cells were lysed by sonication. The protein was first purified by fractionated ammonium sulfate precipitation. In the first step of the precipitation, the concentration of ammonium sulfate was slowly increased to 30%. In the second step, the concentration was raised to 50%. After purification of the sample using hydrophobic interaction chromatography (HIC) and ion exchange chromatography (IEC), the purity index (A_{414}/A_{276}) was up to 0.9 indicating high purity of the protein.

Preparation of Labeled Protein Samples. Singly ^{15}N-labeled and $^{15}N/^{13}C$ doubly labeled bAdx were prepared as follows. One bacterial colony of *E. coli* strain BL21 with plasmid bAdx/pKKHC was grown on M9 plates with 100 mg/L ampicillin for 18 h. One liter of M9 medium with labeled compounds was inoculated with the grown cells, each liter of this medium containing 6 g of Na_2HPO_4, 3 g of KH_2PO_4, 0.5 g of NaCl, 0.25 g of $MgSO_4 \cdot 7H_2O$, 0.16 g of $FeCl_3$, 0.15 g of $CaCl_2 \cdot 2H_2O$, and 0.050 g of thiamine. For uniform ^{15}N labeling, 1 g of glucose, 2.5 g of glycerol (the use of 1 g of glucose and 2.5 g of glycerol per liter M9-media results in highest expression rates), and 1 g of 98% $^{15}NH_4Cl$ were used in the M9 medium; for double labeling, 1 g of 98% $^{13}C_6$-glucose, 2.5 g of 98% $^{13}C_3$-glycerol, and 1 g of 98% $^{15}NH_4Cl$ were used. The culture was incubated at 37 °C with shaking until the OD_{600} reached 0.8. IPTG (150 mg) was added to induce the expression. After 18 h of continuing incubation in a shaker at 37 °C, the bacteria were harvested using centrifugation. The yield of expression was 46 mg of Adx/L of M9 media.

NMR Sample Preparation. About 20 mg of bAdx were used for each NMR sample yielding concentrations of approximately 3 mM. Protein concentrations were determined using $\epsilon_{414} = 11\ mM^{-1}\ cm^{-1}$ (*31*). Amicon stirred cells and YM10 membranes were used to concentrate the protein and to exchange the buffer. Oxidized NMR samples were prepared in 50 mM $NaHPO_4$ buffer (pH 7.4) containing 50 mM NaCl, 10% $^{2}H_2O$, and 2,2-dimethyl-2-sila-pentasulfoneacid (DSS) as standard. Reduction of bAdx with sodium dithionite was prepared as described elsewhere (*32*).

NMR Spectroscopy and Data Processing. NMR experiments were recorded on DMX500 and DMX600 Avance Bruker spectrometers equipped with $^{1}H/^{13}C/^{15}N$ triple-resonance probeheads and pulsed-field-gradient (PFG) accessory. The NMR data sets were collected at 27 °C. The assignment of the protein backbone was based on eight different experiments: HNCA (*33*, *34*), HN(CO)CA (*35*), H(N)CACO, HNCACB (*36*), HNCO (*33*, *37*−*39*), HBHA(CO)NH (*40*), HCACO (*33*), and (HCA)CO(CA)NH (*41*). The side chain assignment was achieved using the 3D (H)CC(O)NH-TOCSY, 3D HCCH-TOCSY (*42*), 3D HNHB (*43*), and 3D TOCSY-(^{15}N,^{1}H)-HSQC (*44*−*48*) experiments. Furthermore, 3D NOESY-(^{15}N,^{1}H)-HSQC and 3D NOESY-(^{13}C,^{1}H)-HSQC experiments (*44*−*48*) were used to collect NOE information. All conditions were the same for oxidized and reduced protein samples.

NMR data were processed on Silicon Graphics workstations with the X-win-NMR software 1.1 (Bruker). ^{1}H chemical shifts were measured relative to internal DSS (taken as 0 ppm). The ^{15}N and ^{13}C chemical shifts were referenced indirectly to DSS by multiplying the spectrometer frequency corresponding to 0 ppm in the ^{1}H spectrum with the $^{15}N/^{1}H$ and $^{13}C/^{1}H$ frequency ratio, respectively, or by the frequency ratio reported by Wishart et al. (*49*).

The homonuclear three bond coupling constant $^{3}J[H^{N}\text{-}H^{\alpha}]$ was determined using a *J*-modulated CT-HMQC experiment (*50*). Nonselective T_1 relaxation times of all detectable ^{1}H protons were determined by the inversion recovery method (*51*). The chemical shift index (CSI) (*52*) was determined for the $^{1}H^{\alpha}$, $^{13}C'$, $^{13}C^{\alpha}$, and $^{13}C^{\beta}$ chemical shifts of oxidized and reduced bAdx.

Structure Calculation. The effect of the paramagnetic center on T_1 times was used to approximately determine distances between single hydrogens and the [2Fe-2S] center (*53*). The self-written program Nmr2st (*54*) was used to automatically find distance constraints. These constraints

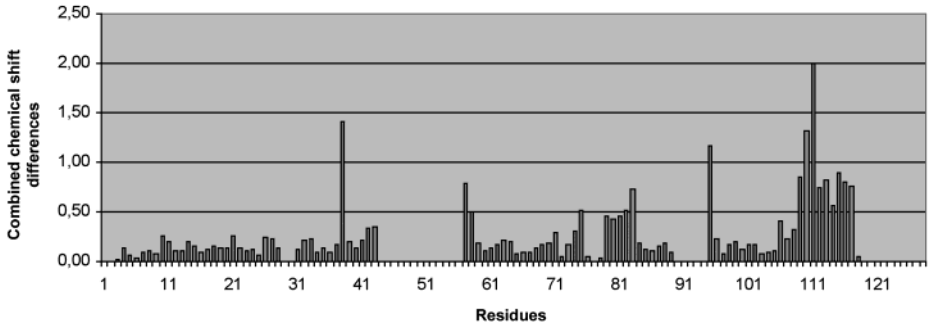

FIGURE 2: The combined chemical shift differences $\Delta\delta_{tot}$ between oxidized and reduced Adx. $\Delta\delta_{tot}$ includes the chemical shift differences of H^N, C^α, H^α, and ^{15}N. The shifts are most pronounced in the C-terminal region. Another region (loop 80−86) that is proposed to be important for protein−protein interactions is also affected.

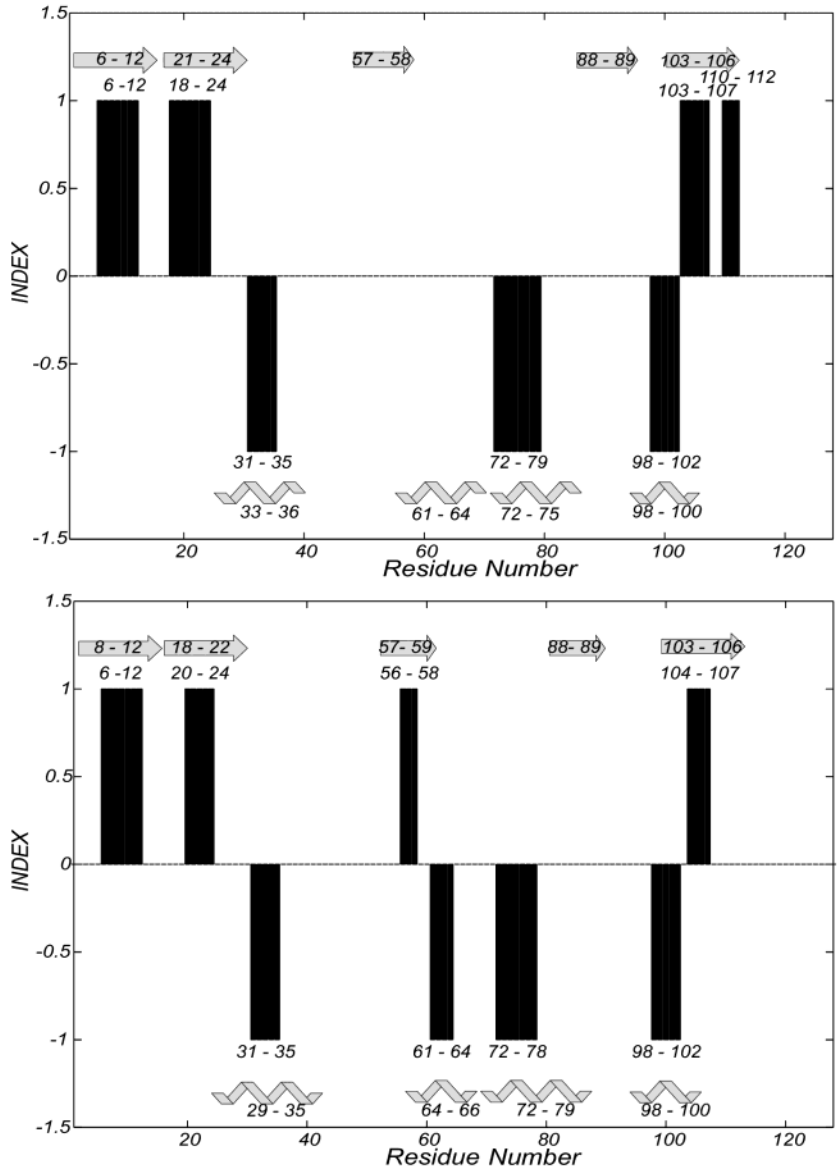

FIGURE 3: Chemical shift index of the reduced (above) and the oxidized state (below). Rectangles upward: β-strands; rectangles downward: α-helix. The secondary structures obtained from NOE data are also indicated (grey symbols). The arrows (above) represent β-strands and the other symbols (below) stand for α-helical secondary structure elements.

were inserted in DYANA version 1.5 (*55*) and used to determine the structure in repeated rounds of distance-based structure calculations. To include the iron−sulfur cluster in the DYANA calculations, it was necessary to define a hypothetical amino acid that contains the iron−sulfur cluster as side chain (*55*).

Cystein 46 was selected as the hypothetical amino acid. Both the distances of sulfur and iron atoms and the distances to the adjacent sulfur atoms of the other three cysteines (C52, C55, and C92) were obtained from the X-ray structure (*22*). The geometry of the iron−sulfur cluster was assumed to be fixed.

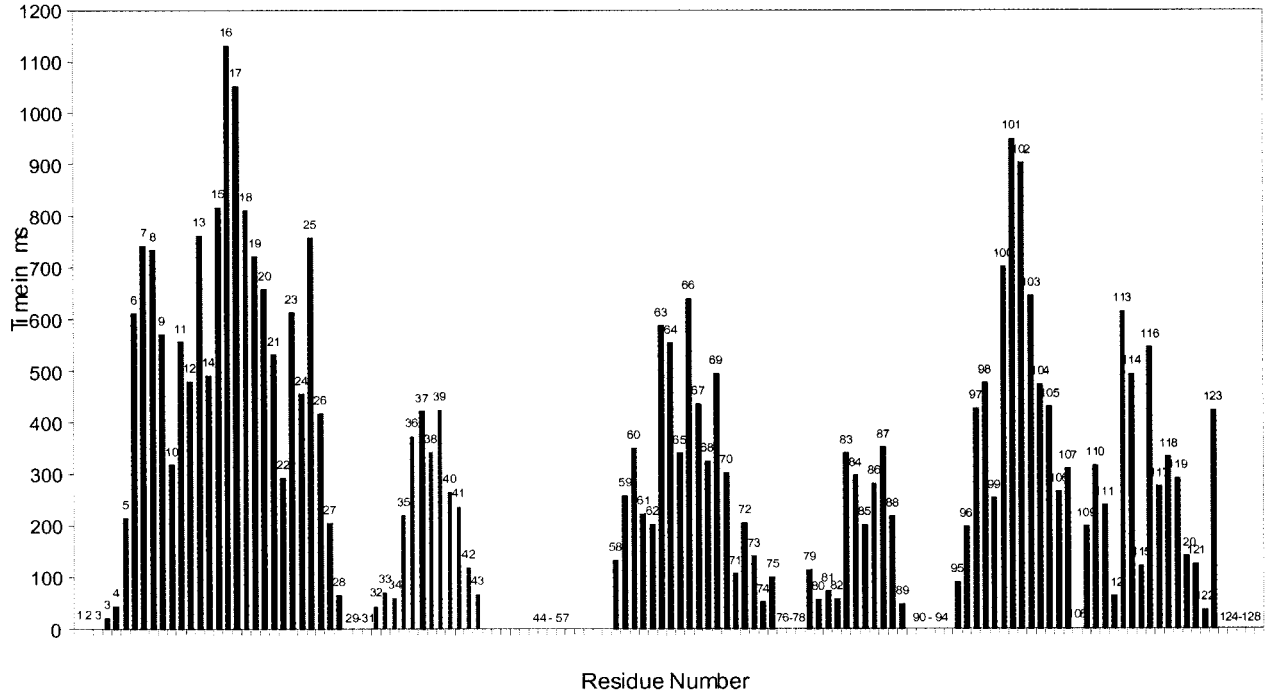

FIGURE 4: T_1 times of the reduced state. Close to the [2Fe-2S] cluster the relaxation times clearly decrease. Regions 29−31, 44−57, 76−78, and 90−94 could not be assigned due to the paramagnetic properties of the [2Fe-2S] cluster.

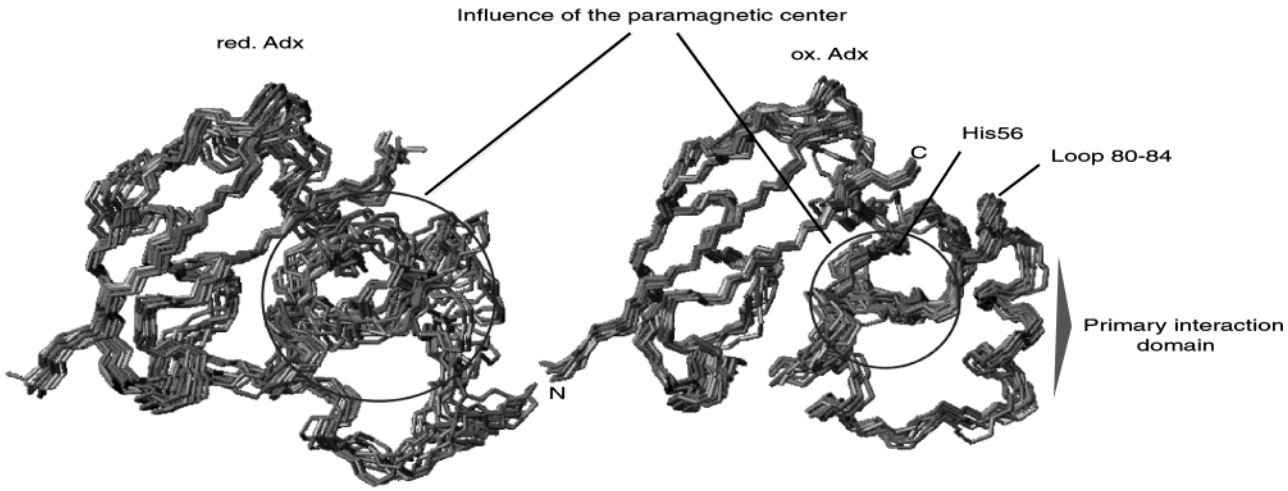

FIGURE 5: Superposition of the final 10 calculated NMR structures of reduced (left) and oxidized bAdx (right). Due to paramagnetism, the region around the [2Fe-2S] cluster is not well defined (circle). In the reduced state, paramagnetic effects are more pronounced. Some structurally relevant areas are marked. The figure was generated using MOLMOL (ETH Zürich).

RESULTS

Sequential resonance assignments of bAdx were achieved by the combined analysis of a series of 3D triple resonance experiments including HNCA, HN(CO)CA, H(N)CACO, HNCACB, HNCO, HBHA(CO)NH, HCACO, and (HCA)-CO(CA)NH. The sequential assignments of the side chain resonances were achieved using the 3D (H)CC(O)NH-TOCSY, 3D HCCH-TOCSY, 3D HNHB, 3D TOCSY-(^{15}N,^{1}H)-HSQC experiments. We used 3D-NOESY-(^{15}N,^{1}H)-HSQC and 3D-NOESY-(^{13}C,^{1}H)-HSQC spectra to obtain NOE distance restraints.

The resonances of approximately 70 and 75% of the 128 amino acid residues could be assigned for the reduced and the oxidized bAdx, respectively. Most of the nonassigned residues are located close to the [2Fe-2S] cluster and are affected by its paramagnetism. Comparison of the HSQC spectra of oxidized and reduced bAdx shows that the dispersion of amide resonances in both redox states is satisfactory. The difference in chemical shifts has been determined for the resonances of the H^N, C^α, H^α, and ^{15}N atoms. The combined chemical shift differences $\Delta\delta_{TOT}$ (*56*) are shown in Figure 2. The shifts are most distinct in the C-terminal domain as exemplified by Val 111. The resonances around Tyr 82 also show moderate differences in chemical shift. Chemical shift differences of single residues could be observed for Leu 38 and Leu 57.

Three helices and four β-strands were indicated by the CSI analysis for the oxidized state (Figure 3). After the measurement of selective T_1 times, 86 of the 128 $^3J(H^N,H^\alpha)$ coupling constants could be obtained. On this basis, structural information on the ϕ dihedral angle could be obtained (*57*). For example, values of the coupling constants >8 Hz are

observed in residues Ile7 to Ile12 indicating an extended backbone structure in that region which is possibly part of a β-strand. $^3J(H^N,H^\alpha)$ coupling constants that are smaller than 5 Hz indicate helical structure elements.

The H^α_i-H^N_{i+3} and H^α_i-H^N_{i+4} NOE patterns from the ^{15}N-NOESY-HSQC experiment suggest that helical structures exist in the domains between residues 29−35, 64−69, 72−79, and 98−101 in the oxidized state (Figure 3). As expected, there are no H^α_i-H^N_{i+2} NOEs in α-helical regions (*58*). The situation is similar for the reduced state; however, in this case the third helix is shorter and ranges from residue 72 to 75. These secondary structural elements were also identified for the reduced state except for the β-strand 56−58 and the helix 61−64.

Figure 4 shows the influence of the [2Fe-2S] cluster on T_1 relaxation. The region of residues 29−32, 44−57, 76−78, and 90−94 of the reduced bAdx are strongly affected by the paramagnetism. The distances between single hydrogens and the [2Fe-2S] center are calculated from the r^{-6} dependence of the paramagnetic relaxation rates (*52*). Only H^N protons were used for calculations that are affected by paramagnetism. There is a very good agreement between the distances of reduced bAdx obtained from NMR and the X-ray data (*22*) of the oxidized form, with the exception of Val 32 and Tyr 82.

For both redox states, a structure calculation was carried out with the program DYANA (Figure 5) using about 1300 and 1600 distance constraints for the reduced and oxidized bAdx, respectively. Significant differences are caused by the increased impaired electron-spin density on the metal cluster in reduced relative to oxidized Adx. The coordinates of the two redox states have been deposited in the RCSB Protein Data Bank with PDB ID code 1L6U for the oxidized state and 1L6V for the reduced state. The backbone RMSD values of the final 10 structures are 1.63 ± 0.2 Å and 2.36 ± 0.25 Å for the oxidized and reduced states, respectively. The atomic RMSD of the annealed structures for the backbone is 0.94 ± 0.16 Å for the oxidized state and 1.53 ± 0.22 Å for the reduced state. Both structures differ particularly (Figure 5) in the regions of residues 29−31, 43−55, 76−78, and 90−94 where resonance assignment could not be accomplished because of the proximity to the paramagnetic cluster. However, differences also exist in domains that could be fully assigned. For instance, the loop 80−84 changes its position. The NMR structure of the oxidized state has been superimposed to both the X-ray structure and the NMR structure of the reduced state (Figure 6). The RMSD of backbone atoms is shown in Table 1. The results suggest that the solution structure of oxidized Adx is quite similar to the X-ray structure (the overall RMSD without regions that could not be assigned is 1.23 Å). The largest differences between the two redox states was found in the region 68−85 (RMSD: 3.07 Å). This region includes the primary interaction domain (72−79) as well as the loop 80−84.

DISCUSSION

Due to the paramagnetic properties of bAdx only 70% of the amino acid resonances of the reduced and 75% of the oxidized state could be assigned. The assignment was also complicated by the flexibility of the C-terminus, especially in the oxidized state.

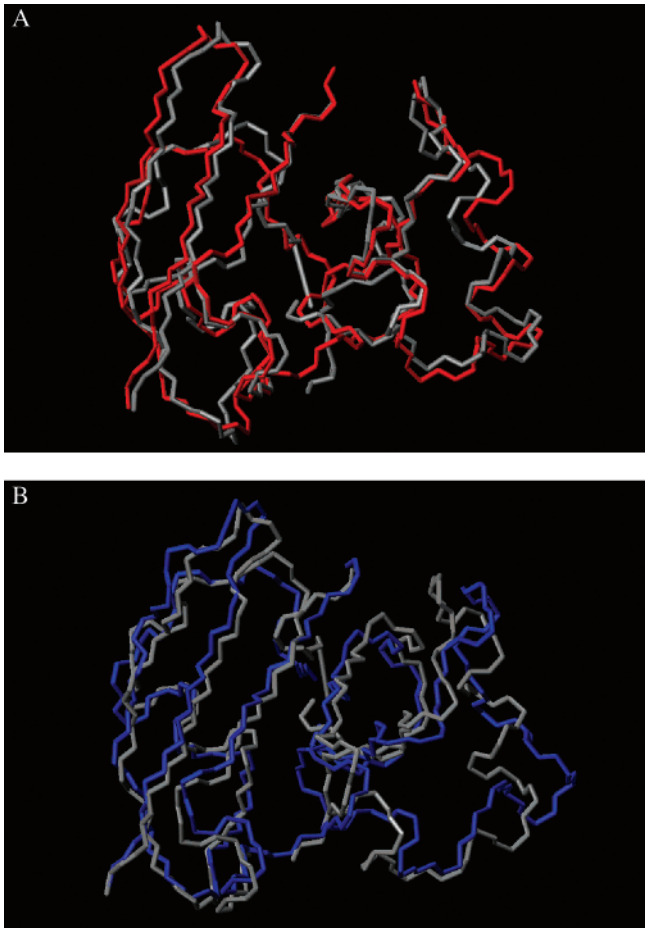

FIGURE 6: (A) Superposition of the backbone atoms of the mean NMR structure (grey) of Adx(ox) and the X-ray (red) structure. The overall fold of the two structures is similar, and the RMSD value is 1.23 Å for the backbone atoms. (B) Superposition of the two solution structures of the reduced (blue) and the oxidized (grey) state of bAdx. The majority of the differences between the two states appear to be in the region 68−85 (RMSD: 3.07 Å). This region includes the primary interaction domain (72−79) as well as the loop 80−86.

Table 1: RMSD Values of Several Regions of Adx[a]

residues	RMSD NMR(ox)/ X-ray(ox)	RMSD NMR (ox/red)
6−40; 57−76; 79−89; 96−108	1.23	2.21
6−25	0.61	0.79
6−40	1.05	1.56
68−76; 79−85	1.23	3.07
85−89; 95−108	0.83	1.51

[a] Column 1 comparison of X-ray and NMR structures in the oxidized state. The RMSD values for regions without the paramagnetic affected backbone atoms are 1.23. Column 2: comparison of the oxidized and reduced states of the solution structures show the largest changes in the interaction domain (68−76; 79−85).

The differences in paramagnetic behavior of the two redox centers must also be taken into account. Differences in chemical shifts are not necessarily caused by structural changes; this is particularly true in the vicinity of the [2Fe-2S] cluster. On the other hand, differences in chemical shifts of atoms which are more than 8 Å distant from the cluster can indicate structural changes upon oxidation/reduction.

Taking this into account, the NMR parameters of the reduced and oxidized states have been compared. Differences

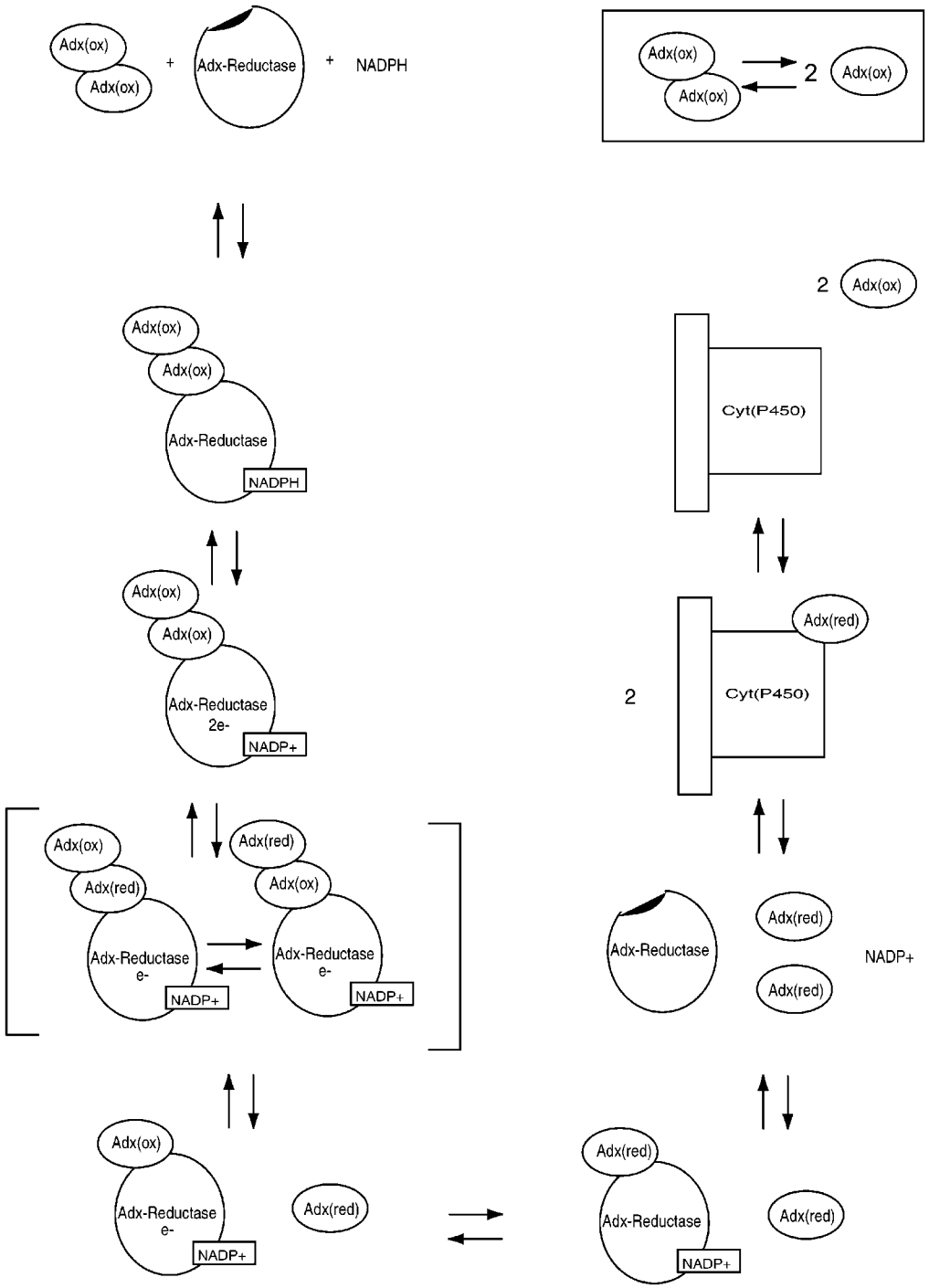

FIGURE 7: Suggested mechanism of interaction of bAdx with Adx-reductase. The Adx(ox) dimer binds to the reductase. One electron is transferred to the Adx bound to the reductase. The electron is then transported to the second Adx molecule which dissociates changing the conformation in the contact domain of the dimer. After reduction, the second Adx dissociates, too. Both Adx(red) monomers are again oxidized by the Cyt P450 system and the Adx(ox) dimer is forming again.

could be observed in the CSI which uses the $^{1}H^{\alpha}$, $^{13}C'$, $^{13}C^{\alpha}$, and $^{13}C^{\beta}$ resonances to predict the secondary structure. In the oxidized state, the involvement of residues 56−58 in a β-strand was indicated in addition to the regions 6−12, 18−24, 103−107 that are also suggested in the reduced state. Here the residues 110−112 were additionally indicated. Furthermore, the helix 61−64 is only predicted in the oxidized state.

Differences between the redox states could also be observed in the NOE patterns. When considering the helix F between the residues 72−79, it must be noted that the resonances of amino acids 77 and 78 could not be observed in NOESY−HSQC spectra of the reduced state. This could be caused by changes of the paramagnetic environment in the different redox states or, more probably, redox-dependent structural changes. After reduction of bAdx by the reductase, the bAdx−AdR complex dissociates, which may be induced by structural changes in the binding domain containing the helix 72−79. A decrease in distance between the metal cluster and residues 77−78 could be the reason sequential connectivities are not observed. Additionally, the helix 29−35 is shortened in the reduced state.

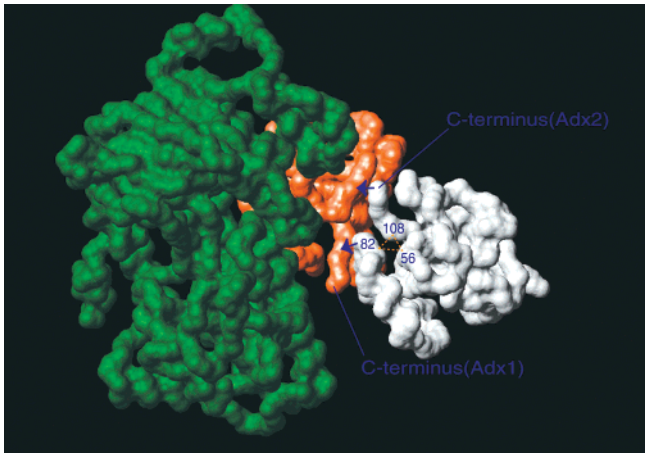

FIGURE 8: To demonstrate that a 1:2 complex may be formed, the X-ray structure [14] of the Adx-dimer (Adx1(pink)−Adx2(grey)) was superimposed to the X-ray structure (*70*) of the reductase-Adx (Adr(green)−Adx1(pink)) complex (Figure 8). As can be seen, interactions between the unbound Adx2 and the reductase are unlikely due to the large distance between them favoring the formation of a 1:2 complex at low concentrations of Adx. The triangle indicates hydrophobic interaction between Tyr82 and Pro108 and a hydrogen-bond between His56 and Tyr82 in the oxidized state. Redox dependent movements are represented by arrows. The break of the hydrogen bond between His56 and Tyr82 results in a movement of the loop around Tyr82. This movement leads to a conformational change of the C-terminal part pushing off the second Adx molecule. The figure was generated using MOLMOL (ETH Zürich).

When comparing the chemical shifts of resonances in both redox states significant differences are observed in residues 38, 57, 75, 81−83, 95, and the C-terminal region (Figure 2). Our findings agree very well with the results of other groups (*27*, *32*). Tyr82 is probably involved in protein−protein interactions (*27*, *59*). As already suggested (*22*, *27*), the reduction of Adx may result in a breakdown of the hydrogen bond between His56 and Tyr82. This change could be transferred to the primary interaction domain (Asp72−Asp79; helix F). We also suppose that the change of the redox state results in a breakdown of the hydrogen bond between His 56 and Tyr 82. The loop from 80 to 86 changes its position. Most likely, the helix F is stabilized by this loop in the oxidized state. In the reduced state, this helix is shortened resulting in a change of the position of Asp 79. This change may induce the dissociation of the complex between AdR and Adx. There exist hydrophobic interactions between Tyr82 and Pro108 that are not influenced by the redox switch. This could be the reason for the redox-dependent movement of the C-terminal part.

Structural changes in the region of Tyr 82 may also explain the differences in chemical shifts of the oxidized and reduced state. The chemical shift variations indicate that the C-terminus is the most affected region connected with the change of the Adx redox state. Similar changes were also observed in other ferredoxins such as human ferredoxin (*32*) and putidaredoxin (*60*). It is assumed that these changes are important for the interaction with the corresponding cytochromes. This assumption is supported by mutagenesis studies (*61*, *62*).

The structural features of the oxidized state are well defined and very similar to the X-ray structure. In the evaluation of the reduced protein structure, about 10% less constraints were available especially in structurally relevant central domains. These differences are connected with the increased paramagnetism of the metal cluster in reduced relative to oxidized bAdx. After refinement of the structures, RMSD values of 2.36 ± 0.25 for the reduced and 1.63 ± 0.2 for the oxidized state have been obtained for all heavy atoms. The best 10 structures of the oxidized and reduced states were analyzed using the PROCHECK procedure (*63*); in the Ramachandran plot, 0.6% of all residues are located in disallowed regions of the oxidized state, and about 4% in those of the reduced state. For that reason, the structure of the reduced state determined using the DYANA program must be viewed with caution especially for the regions close to the iron sulfur cluster. However, comparing both redox states a significant structural difference in the interaction domain can be derived.

According to the present work, the reduction of the [2Fe-2S] cluster results in structural changes of the protein. Such redox-dependent changes were also described for human ferredoxin (*32*), putidaredoxin (*60*), and bAdx (*27*). To our knowledge, a comparison of the X-ray structures of ferredoxins in both redox states has been reported in one single case only (*64*), mainly because of extreme difficulties in handling of the protein in the unstable reduced state.

It has been indicated by Pikuleva et al. (*14*) that Adx is essentially present as a dimer at low concentrations. Using dynamic light scattering, a molecular weight of 22.7 kDa was found at concentrations of 97 μM Adx and 10 mM potassium phosphate indicating that Adx is primarily forming a dimer. At concentrations of 779 μM and 10 mM potassium phosphate, the molecular weight decreases to 16 kDa (*14*). The dissociation of the dimer at higher concentrations was explained with repulsive forces between the highly acidic Adx molecules which begin to dominate when the concentration of the protein in solution is increased. The dimer does not affect the NMR measurements as concentrations of Adx are in the millimolar range (2−3 mM). In its natural environment, however, one must assume that a dimer exists in the oxidized state due to lower concentrations in the mitochondrial matrix. Changes of redox state result in conformational changes in the contact region of the dimer, especially in the C-terminal region. These results lead to the conclusion that the dimer either dissociates, or the Adx(red) molecules change their position relative to each other upon reduction. Another reason for the dissociation may be the participation of the C-terminus in the binding to some Cyt P450 species (*61*, *62*). In the case of a dimer, the C-terminal part would not be freely accessible.

Electron Transport Mechanism. The assumption of a 1:2:1 complex formation of AdR, two Adx molecules, and the cytochrome appears unlikely in connection with structural changes between both redox states. According to other reports (*65*, *66*, *68*), such a quarternary complex is also unlikely to occur. In addition, it has been shown that a 1:1 complex is formed between Adx and cytochrome (*66*).

A series of experimental data have suggested that the organized 1:1:1 complex between the reductase, the Adx, and the cytochrome is also unlikely to occur (*65*, *67*, *68*). The high degree of overlap of the two recognition sites clearly rules out the formation of a functional ternary complex involving AdR, Adx, and the cytochrome (*67*).

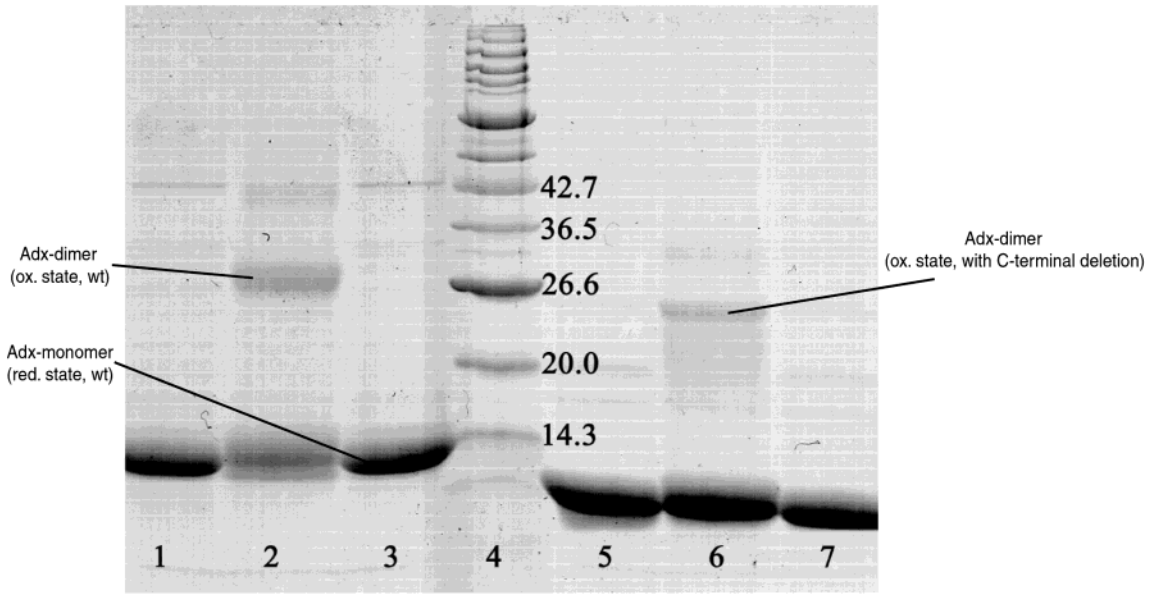

FIGURE 9: Cross-linking experiments of oxidized and reduced bAdx. Lane 1 of the SDS gel shows the full-length oxidized bAdx. The oxidized and reduced full-length bAdx are cross-linked and shown in lanes 2 and 3. The oxidized state is mainly present as a dimer, whereas monomers only occur in the reduced state. The same experiments were performed with Adx-(4−108) mutants (lanes 5−7). These data show that the c-terminus is of particular importance for the dimerization process.

As a result, the following mechanism for electron transport is suggested (Figure 7). The Adx(ox) dimer is preferentially formed in equilibrium with the Adx(ox) monomer. The reductase receives NADPH, which transfers a hydride ion to produce NADP(+) and FADH(−). The docking process displaces Tyr 331 and Arg 124 in the reductase (*69*). The Adx dimer binds to the reductase. FADH(−) transfers one electron to the Adx(1) bound to the reductase as described by Müller et al. (*70*). Then the electron is transported to the second Adx(2) molecule, which is not bound to the reductase (*14*). The reduced Adx(2) dissociates changing the conformation in the contact domain of the dimer. FADH* transfers the second electron to the second Adx(1) molecule which is still bound to the reductase. After reduction, the second Adx-(1) dissociates changing the conformation of helix F. Both Adx(red) monomers are again oxidized by the Cyt P450 system and the Adx(ox) dimer is reconstructed.

The question remains why Adx molecules (one electron transporter) dimerize in nature. The transport of two electrons via a dimer can proceed much faster than via two monomers. If the monomer is acting as a shuttle, the second Adx could only bind when the first one is dissociated. These two steps (dissociation and binding) would need additional time, which could be avoided with dimers. Additionally, the preceding equilibrium between monomer and dimer could play an important role. For example, the use of electrons for steroid hormone production would take place via a complicated regulation system (*71*) in which cAMP is involved. When NADPH concentration increases, dimers of Adx(ox) are reduced to Adx(red) resulting in a decrease of Adx(ox) concentration. The ratio between dimer and monomer is changed toward the dimer, i.e., electrons can be transported faster and more effectively. If only monomers were present, a decrease of the Adx(ox) concentration could not be compensated immediately. In case of reduction, the purpose of the dissociation of the dimer could be to maintain the equilibrium. In the oxidized state, the equilibrium between monomer and dimers possibly serves to regulate the transfer rate of electrons. In case of high adrenodoxin concentrations, monomers are supposed to increase the extent of electron transport. The rate is determined by the excessive supply of oxidized Adx. To maintain the rate of electron transport at low concentrations dimers are preferentially used for electron transfer.

It was shown that oxidized Adx inhibits cholesterol side chain cleavage by competition (*68*). At low concentrations, the dimerization process of Adx could prevent the inhibition of cytochrome.

A precondition for the suggested mechanism is a 1:2 complex formation between the reductase and the Adx-dimer. To demonstrate that a 1:2 complex may be formed, the X-ray structure (*14*) of the Adx-dimer (Adx1−Adx2) was superimposed to the X-ray structure (*70*) of the reductase-Adx (Adr−Adx1) complex (Figure 8). As indicated, interactions between the unbound Adx and the reductase are unlikely due to the large distance favoring the formation of a 1:2 complex at low concentrations. The X-ray structure determination of AdR−Adx complex was carried out at high protein concentrations according to the conditions of crystallization. Presumably under these conditions, no 1:2 complex formation was observed. The break of the hydrogen bridge between His56 and Tyr82 results in a movement of the loop around Tyr82. This movement leads to a conformational change of the C-terminal part pushing off the second Adx molecule (Figure 8).

To find out whether reduced Adx(ox) dimers dissociate by reduction as we suppose, the behavior of the reduced state was investigated at low concentrations. Native SDS−gel electrophoresis and gel-filtration showed that no dimer can be detected under these conditions, which would be in favor of our model. To further prove these findings, cross-linking experiments were performed. These experiments have clearly shown that dimers are mainly present in the oxidized state while only monomers are observed in the reduced state (Figure 9). On the basis of investigations of the Adx(4−108) mutant, it could be shown that the C-terminus is

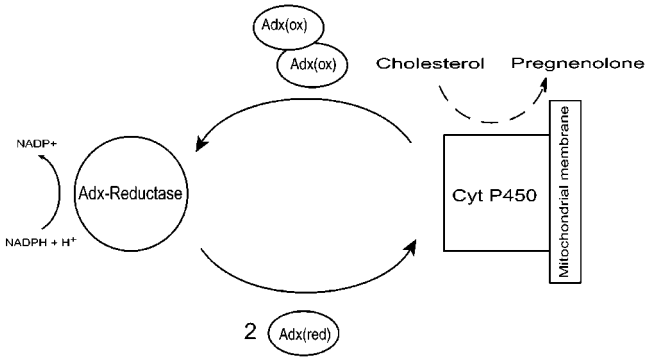

FIGURE 10: Possible electron transport mechanism: Adx (ox) dimers are reduced by the Adx-reductase. The redox-dependent changes especially in the C-terminal region of Adx result in a dissociation of the dimer. The two Adx(red) monomers are again oxidized by the Cyt P450 system.

essential for the dimerization process (Figure 9). These data confirm the suggested mechanism. Summarizing the results of the present work, the shuttle model suggested by Lambeth et al. (*11*) could be confirmed. It must be emphasized, however, that electron transport can take place via both a monomer or a dimer species (Figure 10). Dimers are preferentially formed in the oxidized state. Significant conformational changes, especially in the C-terminal region, lead to the dissociation of the Adx dimer upon reduction.

The process of steroid synthesis must occur quickly and effectively. In mitochondrial steroid hydroxylase systems, adrenodoxin dimers serve to optimize the reaction. The dissociation of the dimer upon reduction accelerates the electron transport.

REFERENCES

1. Grinberg, A. V., Hannemann, F., Schiffler, B., Müller, J., Heinemann, V., and Berhardt, R. (2000) *Proteins 40*, 590−612.
2. Xia, B., Cheng, H., Skjeldahl, L., Coghlan, V. M., Vickery, L. E., and Markley, J. L. (1995) *Biochemistry 34*, 180−187.
3. Stormer, F. C., Pedersen, J. I., and Oftebro, H. (1979) *J. Biol. Chem. 254*, 4331−4334.
4. Kimura, T., and Suzuki, K. (1965) *Biochem. Biophys. Res. Commun. 19*, 340−345.
5. Cupp, J. R., Vickery, L. E., and Coghlan, V. M. (1988) *Arch. Biochem. Biophys. 264*, 376−382.
6. Kimura, T. (1968) *Struct. Bonding 5*, 1−40.
7. Saarem, K., Bjorkhem, I., Pedersen, J. I., and Oftebro, H. (1981) *J. Lipid. Res. 22*, 1254−1264.
8. Okuda, K., and Atsuta, Y. (1978) *J. Biol. Chem. 253*, 4653−4658.
9. Hiwatashi, A., Ichikawa, Y., and Waki, N. (1986) *FEBS Lett. 195*, 87−91.
10. Lambeth, J. D., and Kamin, K. (1979) *J. Biol. Chem. 254*, 2766−2774.
11. Lambeth, J. D., Seybert, D. W., Lancaster, J. R., Salerno, J. C., and Kamin, H. (1982) *Mol. Cell. Biochem. 45*, 13−31.
12. Kido, T., and Kimura, T. (1979) *J. Biol. Chem. 254*, 11806−11815.
13. Hara, T., and Takeshima, M. (1994) *Cytochrome P450 8th Int. Conf.* 417−420.
14. Pikuleva, I., Tesh, K., Waterman, M. R., and Kim, Y. (2000) *Arch. Biochem. Biophys. 373*, 44−55.
15. Uhlmann, H., Beckert, V., Schwarz, D., and Bernhardt, R. (1992) *Biochem. Biophys. Res. Commun. 1188*, 1131−1138.
16. Poe, M., Phillips, W. D., McDonald, C. C., and Lovenberg, W. (1970) *Proc. Natl. Acad. Sci. U.S.A. 65*, 797−804.
17. Brinzinger, H., Palmer, G., and Sands, R. H. (1966) *Proc. Natl. Acad. Sci. U.S.A. 55*, 397.
18. Watari, H., and Kimura, T. (1966) *Biochem. Biophys. Res. Commun. 24*, 106.
19. Kimura, T., Tasaki, A., and Watari, H. (1970) *J. Biol. Chem. 254*, 4450−4452.
20. Gibson, J. F., Hall, D. O., Thornley, J. H. M., and Whatley, F. R. (1966) *Proc. Natl. Acad. Sci. U.S.A. 56*, 987.
21. Lammack, R., Rao, K. K., Hall, D. O., and Johnson, C. E. (1971) *Biochem. J. 125*, 849−856.
22. Müller, A., Müller, J. J., Muller, Y. A., Uhlmann, H., Bernhardt, R., and Heinemann, U. (1998) *Structure 6*, S. 269−280.
23. Suhara, K., Takemori, S., and Katagiri, M. (1972) *Biochim. Biophys. Acta 263*, 272−278.
24. Marg, A., Kuban, R.-J., Behlke, J., Dettmer, R., and Ruckpaul, K. (1992) *J. Mol. Biol. 227*, 945−947.
25. Greenfield, N. J., Wu, X., and Jordan, F. (1989) *Biochim. Biophys. Acta 995*, 246−254.
26. Miura, S., and Ichikawa, Y. (1990) *J. Biol. Chem. 266*, 6252−6258.
27. Miura, S., Tomita, S., and Ichikawa, Y. (1991) *J. Biol. Chem. 266*, 19212−19216.
28. Beckert, V., Schrauber, H., Bernhardt, R., Van Dijk, A., Kakoschke, C., and Wray, V. (1995) *Eur. J. Biochem. 231*, 226−235.
29. Weiss, R., Brachais, L., Löhr, F., Hartleib, J., Bernhardt, R., and Rüterjans, H. (2000) *J. Biomol. NMR 17*, 355−356.
30. Porter, T. D., and Larson, J. R. (1991) *Methods Enzymol. 206*, 108.
31. Huang, J. J., and Kimura, T. (1973) *Biochemistry 12*, 406−409.
32. Xia, B., Cheng, H., Skjeldahl, L., Coghlan, V. M., Vickery, L. E., and Markley, J. L. (1998) *Biochemistry 34*, 180−187.
33. Kay, L., Ikura, M., Tschudin, R., and Bax, A. (1990) *J. Magn. Reson. 89*, 496−514.
34. Farmer, B., II, Venters, R., Spicer, L., Wittekind, M., and Müller, L. J. (1992) *J. Biomol. NMR 2*, 195.
35. Bax, A., and Ikura, M. (1991) *J. Biomol. NMR 1*, 99.
36. Wittekind, M., and Müller, L. (1993) *J. Magn. Reson. Ser. B 101*, 201.
37. Westler, W., Stockman, B., and Markley, J. (1988) *J. Am. Chem. Soc. 110*, 6256.
38. Mooberry, E., Oh, B., and Markley, J. (1989) *J. Magn. Reson. 85*, 147.
39. Niemczura, W., Helm, G., Chesnick, A., Moore, R., and Bornemann, J. (1989) *J. Magn. Reson. 81*, 635.
40. Grzesiek, S., and Bax, A. (1993) *J. Biomol. NMR, 3*, 185−204.
41. Löhr, F., and Rüterjans, H. (1995) *J. Biomol. NMR, 6*, 189−197.
42. Bax, A., Clore, G., and Gronenborn, A. (1990) *J. Magn. Reson. 88*, 425.
43. Archer, S., Ikura, M., Torchia, D., and Bax, A. (1991) *J. Magn. Reson. 95*, 636−641.
44. Wittekind, M., Gorlach, M., Friedrichs, M., Dreyfuss, G., and Müller, L. (1992) *Biochemistry 31*, 6254.
45. Marion, D., Driscoll, P., Kay, L., Wingfield, P., Bax, A., Gronenborn, A., and Clore, G. (1989) *Biochemistry 28*, 6150.
46. Zuiderweg, E., Mcintosh, L., Dahlquist, F., and Fesik, S. (1990) *J. Magn. Reson. 86*, 210.
47. Consatantine, K., Goldfarb, V., Wittekind, M., Anthony, J., Ng, S., and Müller, L. (1992) *Biochemistry 31*, 5033.
48. Fairbrother, W., Palmer, A., III., Rance, M., Seizer, J., Saier, H., and Wright, P. (1992) *Biochemistry 31*, 4413.
49. Wishart, D. S., Bigam, C. G., Yao, J., Abildgaard, F., Dyson, H. J., Oldfield, E., Markley, J. L., and Sykes, B. D. (1995) *J. Biomol. NMR 6*, 135−140.
50. Kubovina, H., Grzesiek, S., Delaglio, F., and Bax, A. (1994) *J. Biomol. NMR 4*, 871−878.
51. Bentrop, D., Bertini, I., Cremonini, M. A., Forsén, S., Luchinat, C., and Malmendal, A. (1997) *Biochemistry 36*, 11605−11618.
52. Wishart, D. S., and Sykes, B. D. (1994) *J. Biomol. NMR 4*, 171−180.
53. Bertini, I., Couture, M. M. J., Donaire, A., Eltis, L. D., Felli, I. C., Luchinat, C., Piccioli, M., and Rosato, A. (1996) *Eur. J. Biochem. 241*, 440.
54. Pristovsek, P., Lücke, C., Reincke, B., Ludwig, B., and Rüterjans, H. (2000) *Eur. J. Biochem. 267*, 4205−4212.

55. Güntert, P., Mumenthaler, C., and Wüthrich, K. (1997) *J. Mol. Biol. 273*, 283−298.
56. Ayed, A., Mulder, F. A. A., Yi, G.-S., Lu Y., Kay L. E., and Arrowsmith, C. H. (2001) *Nat. Struct. Biol. 8*, 756.
57. Karplus, M. (1963) *J. Am. Chem. Soc. 85*, 2870−2871.
58. Wüthrich, K., Billeter, M., and Braun, W. (1984) *J. Mol. Biol. 180*, 715−740.
59. Beckert, V., Dettmer, R., and Bernhardt, R. (1994) *J. Biol. Chem. 269*, 2568−2573.
60. Pochapsky, T. C., Ratnaswarny, G., and Patera A. (1994) *Biochemistry 33*, 6433−6441.
61. Uhlmann, H., Kraft, R., and Bernhardt, R. (1994) *J. Biol. Chem. 269*, 36, 22557−22564.
62. Schiffler, B., Kiefer, M., Wilken, A., Hannemann, F., Adolph, H. W., and Bernhardt, R. (2001) *J. Biol. Chem. 276*, 36225−36232.
63. Laskowski, R. A., MacArthur, M. W., Moss, D. S., and Thoraton, J. M. (1993) *J. Appl. Crystallogr. 26*, 283−291.
64. Morales, R., Chron, M.-H., Hundry-Clergeon, G., Petillot, Y., Norager, S., Medina, M., and Frey, M. (1999) *Biochemistry 38*, 15764−15773.
65. Schwarz, D., Chernogogolov, A., and Kisselev, P. (1999) *Biochemistry 38*, 9456−9464.
66. Takeuchi, K., Tsubaki, M., Futagawa, J., Masuya, F., and Hori, H. (2001) *J. Biochem. 130*, 789−797.
67. Vickery, L. E. (1997) *Steroids 62*, 124−127.
68. Hanukoglu, I., and Jefcoate, C. R. (1980) *J. Biol. Chem. 255*, 3057−3061.
69. Ziegler, G. A., and Schulz G. E. (2000) *Biochemistry 39*, 10986−10995.
70. Müller, J. J., Lapko, A., Bourenkov, G., Ruckpaul, K., and Heinemann, U. (2001) *J. Biol. Chem. 276*, 2786−2789.
71. Stocco, D. M. (2000) *Biochim. Biophys. Acta 1486*, 184−197.

BI0160361